Geophys. J. Int. (2004) **157,** 1152–1162 doi: 10.1111/j.1365-246X.2004.02233.x

PP-P differential traveltime measurement with crustal correction

Masayuki Obayashi,[1] Daisuke Suetsugu[1] and Yoshio Fukao[1,2]

[1] *Institute for Frontier Research on Earth Evolution, JAMSTEC, Yokosuka, Japan. E-mail: obayashi@jamstec.go.jp*
[2] *Earthquake Research Institute, University of Tokyo, Tokyo, Japan*

Accepted 2003 December 23. Received 2003 December 23; in original form 2002 November 7

SUMMARY

PP-P differential traveltime data are useful for constraining the seismic structure of the upper mantle. The cross-correlation method has been used for these measurements, whereby a synthetic *PP* waveform is constructed from the observed *P* and is cross-correlated with the observed *PP*. *PP* waveforms are, however, distorted by interference with the precursors and post-cursors produced by reflections and conversions at crustal discontinuities. Accordingly, the measurement of *PP-P* differential traveltimes can suffer a bias. Synthetic experiments have shown that this bias becomes significant when seismograms are lowpass filtered. To measure *PP-P* differential times without such bias, we developed a method to take crustal effects into consideration in the cross-correlation method. In this new method, the response of incident *P* to the crustal structure beneath the *PP* bounce point is calculated and convolved with the observed *P* in constructing the synthetic *PP* waveform. As an experiment we applied this to real seismograms lowpass filtered with corners at 0.5, 0.1 and 0.05 Hz. We took crustal models from the global database CRUST2.0. This experiment shows that the method is effective in reducing the bias in traveltime measurements, even for measurements with long period waveforms below 0.05 Hz. With the assumption that the crustal structure is described by CRUST2.0, the application of our method to the observed seismograms provides *PP-P* values mutually consistent among the measurements using three different lowpass filters with corners at 0.5, 0.1 and 0.05 Hz.

Key words: body waves, crustal structure, Earth's interior, *PP-P*.

1 INTRODUCTION

PP waves are useful for investigating the upper mantle structure in the region that few direct *P* waves sample. Woodward & Masters (1991) and Masters *et al.* (2000) measured *PP-P* differential traveltimes from long-period seismograms by cross-correlating the waveforms between the observed *PP* and synthetic *PP* calculated from the observed *P*. They related the measured *PP-P* values to the upper-mantle structures beneath the *PP* bounce points. Fukao *et al.* (2003) also measured *PP-P* times using a similar method on broad-band seismograms with 0.5 Hz lowpass filtering and incorporated them with direct *P* traveltimes for whole mantle tomography. Paulssen & Stutzmann (1996), however, measured *PP-P* times using the same method on both broad-band and long-period data and found discrepancies of more than 1-s between them. The interference of the *PP* phase with secondary arrivals was considered to be a cause of the incoherent measurement. Fukao *et al.* (2003) indicated that it is important to take the sea-water reverberation into account when the *PP* rays bounce under oceans. Fukao *et al.* (2003), furthermore, pointed out that lowpass filtering tends to make *PP-P* times systematically shorter because of interference of the *PP* with its precursors and post-cursors as a result of reflections and conversions at crustal discontinuities. To avoid the contamination of these precursors and post-cursors into the main *PP* waveform, they adopted a relatively high cut-off of 0.5 Hz for lowpass filtering. The use of the 0.5 Hz lowpass filter, however, limits the availability of waveform data because of large background noise in the frequencies from 0.1 to 1 Hz. Lowpass filtering with a corner at a lower frequency would reduce the background noise and allows us to obtain a larger number of *PP-P* data.

In this paper, we introduce a new procedure to account for the crustal response at a *PP* bounce point by synthesizing the *PP* waveform from an observed *P* waveform. We demonstrate that the method is useful in reducing the bias caused by crustal reverberation for a broad frequency range from 0.05 to 0.5 Hz and that the correction may reach up to a few seconds, which is significant for the measurement of *PP-P* differential traveltimes and tomographic models resulting from *PP-P* time data.

2 METHOD OF *PP-P* MEASUREMENT

Our measurement of *PP-P* differential times is similar to those of the previous studies (e.g. Woodward & Masters 1991; Fukao *et al.* 2003) in which a synthetic *PP* waveform was calculated from the observed *P* waveform and cross-correlated with the observed *PP* waveform. A synthetic *PP* waveform is obtained by:

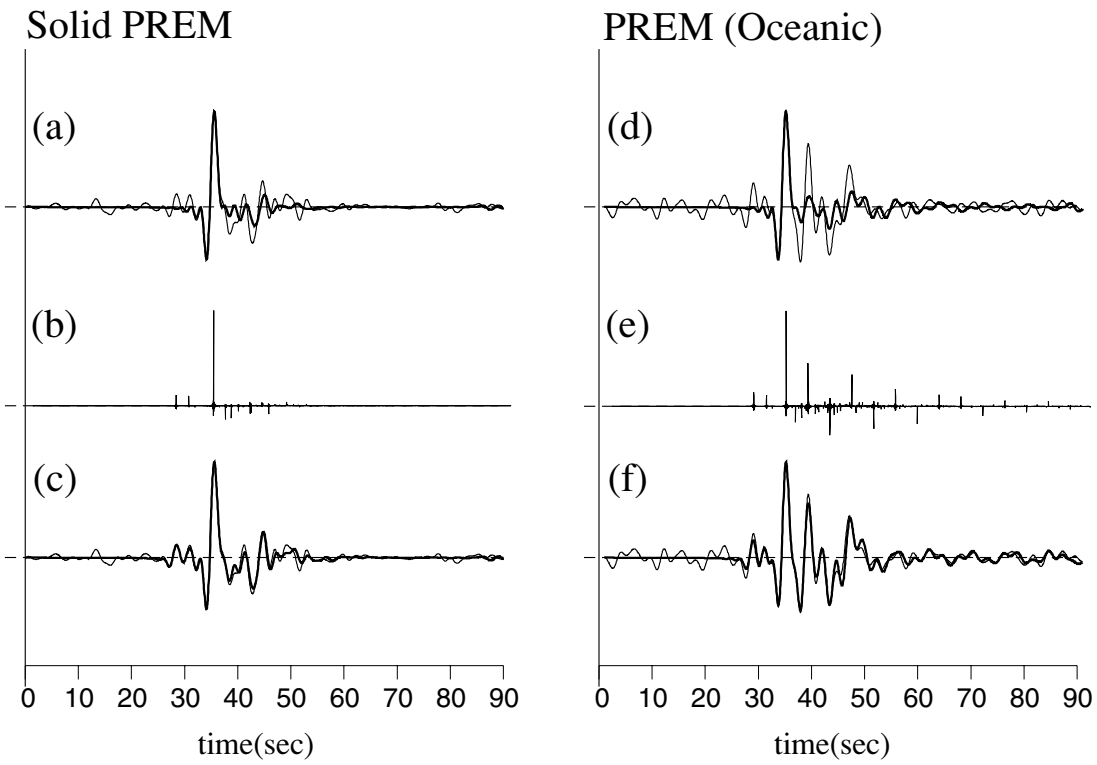

Figure 1. Synthetic *PP* waveforms constructed from the observed *P* waveform, where synthetic seismograms by DSM (Takeuchi *et al.* 1996) are regarded as observed seismograms. The synthetic *PP* waveform without the crustal correction (a and d) and with the crustal correction (c and f) are represented by thick lines and are superposed on the observed *PP* waveform (thin line) after having shifted the synthetic *PP* waveforms in time by the *PP-P* times predicted from ray theory. The synthetic *PP* waveforms with the crustal correction were made by convolving the uncorrected synthetic *PP* waveforms with the crustal responses for the reflections (b and e). Two observed seismograms were calculated for PREM (right column) and solid PREM (left column), for which crustal structures are shown in Table 1.

(i) lowpass filtering an observed seismogram,
(ii) windowing the *P* waveform,
(iii) applying the Hilbert transform,
(iv) convolving with the crustal response at the *PP* bounce point,
(v) applying a t^* operator to account for different attenuation along the *P* and *PP* raypaths,
(vi) correcting for the polarities of *P* and *PP* resulting from focal mechanism.

Step (iv) is the new procedure introduced in this study.

The response for a layered crustal (and sea water, if necessary) structure is first calculated at the bounce point using the Haskell matrix method (Haskell 1962). We define the crustal response as the waveform of *P* outgoing from the Moho in response to the *P*-wave impulse incident to the Moho beneath the bounce point. The crustal response function is shifted in time so that the reflection at the top of the crustal model (the boundary between the solid and sea water/air) has no phase lag. Next, we convolve the crustal response with the waveform obtained at step (iii). We refer to the procedure at step (iv) as crustal correction.

Fig. 1 explains the crustal correction using synthetic seismograms for the Preliminary Refernce Earth Model (PREM) (Dziewonski & Anderson 1981) and for a modified PREM in which the sea water layer was replaced with an upper crust layer (hereafter called solid PREM). The crustal structures of these models are shown in Table 1. The synthetic seismograms were calculated by the direct solution method (DSM) (Takeuchi *et al.* 1996) in a frequency range up to 1 Hz. The source was an isotropic expansion

Table 1. Crustal structures for synthetic seismograms.

	Sea water	Upper crust	Lower crust
V_P (km s^{-1})	1.45	5.80	6.80
V_S (km s^{-1})	0.0	3.20	3.90
ρ (g cm^{-3})	1.02	2.60	2.90
Thickness (km)			
PREM	3.0	12.0	9.4
Solid PREM	0.0	15.0	9.4

V_P, V_S and ρ represent *P*-wave velocity, *S*-wave velocity and density, respectively.

at 500 km depth and the epicentral distance was 76°. As for the PREM, the station was assumed to be settled at the bottom of the ocean (on the solid surface). The synthetic seismogram is regarded as an observed seismogram in the experiment. Figs 1(a) and (d) show synthetic *PP* waveforms (thick lines) constructed from the observed *P* waveforms by the ordinary method (i.e. by applying above steps (i)–(v), excluding (iv)). These are superposed on the observed *PP* waveforms (thin lines) after having been shifted in time by the predicted *PP-P* differential times. Although the main phase of the synthetic *PP* agrees with the observed *PP*, there are discrepancies at the precursor and post-cursor portions corresponding to the crustal reverberations. Figs 1(c) and (f) show the waveforms obtained by convolving these synthetic *PP* waveforms with the crustal responses (Figs 1b and e). The crustal responses were calculated for the same crustal structure used in making the synthetic seismograms (Table 1). The synthetic *PP* waveforms

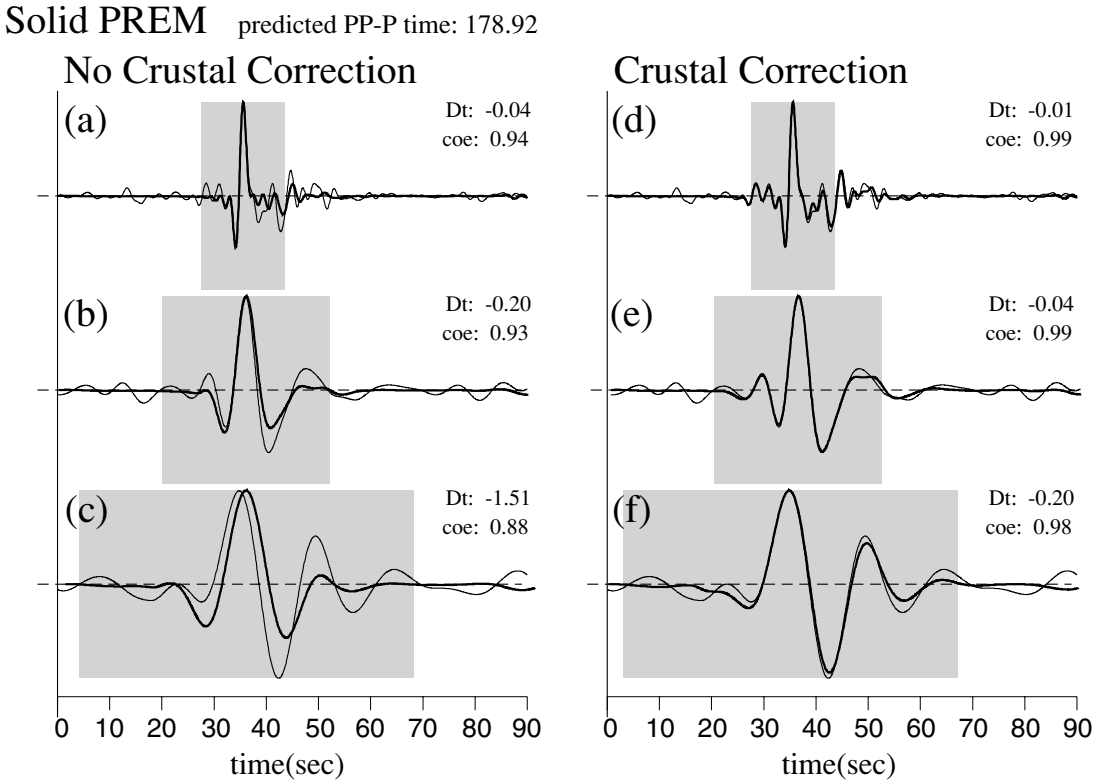

Figure 2. Apparent time-shifts as a result of interferences by the crustal reverberations with the main *PP* waves. The synthetic *PP* waveform (thick line) and observed *PP* waveform (thin line) with respect to the solid PREM in Figs 1(a) and (c) are shown in left and right columns, respectively, after lowpass filtering with three different corner frequencies (top, middle and bottom are 0.5, 0.1 and 0.05 Hz, respectively). Shaded portions indicate the windows for cross-correlation. The measured *PP-P* residuals and maximum correlation coefficients are shown at the top and bottom of each diagram, respectively.

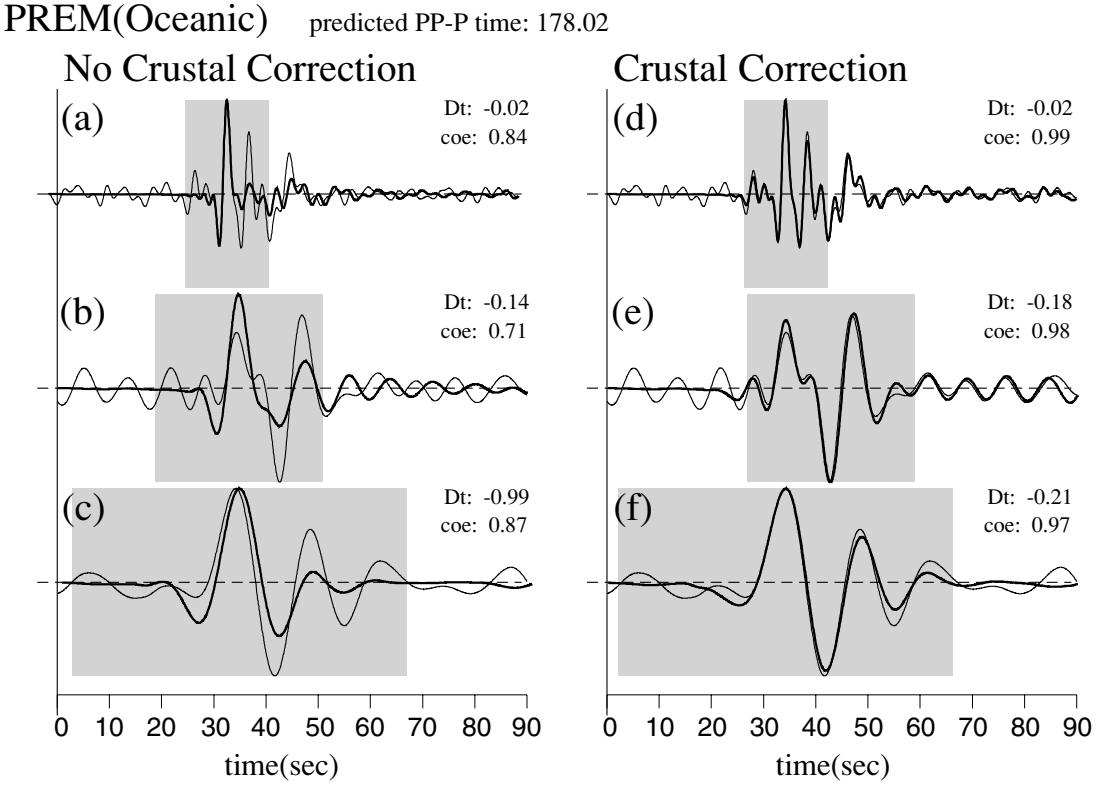

Figure 3. Same as Fig. 2, however, for waves with respect to the PREM in Figs 1(d) and (f).

with the crustal corrections agree well with the observations, including the precursors and post-cursors. Slight differences are still observed because of the difference in the incident angles between *P* and *PP*, which caused a trifling disparity in the crustal response under the station. The *PP* waveform can be reconstructed completely if the observed *P* waveforms are preprocessed by deconvolving the crustal response of the *P* wave incident to the crust under the station and convolving that of the *PP* wave. However, this procedure is not practical for real measurements because this effect is subtle relative to the influence of the uncertainty in the crustal structure under the station.

Poor reconstructions of the precursor and post-cursor in the synthetic *PP* waveform without the crustal corrections induce a significant bias in *PP-P* time measurement if the waveform is lowpass filtered (Fukao *et al.* 2003). Figs 2 and 3 show the lowpass filtered *PP* waveforms with three different corners at 0.5, 0.1 and 0.05 Hz from top to bottom, for the solid PREM and the PREM, respectively. Shown at the top right of each diagram is the *PP-P* time residual (Δt) measured using the cross-correlation method. The window for the cross-correlation (shade area) was fixed on the synthetic *PP* waveform so that the time of maximum amplitude was centered in it and its width varied according to corner frequency of lowpass filtering (16, 32 and 64 s for 0.5, 0.1 and 0.05 Hz corner frequencies, respectively). The synthesis was superposed on the observation after having been shifted in time by the predicted *PP-P* time. The correlation coefficient had a maximum, which was also shown at the top right of each diagram, after the synthesis is shifted in time by Δt. We obtained six values of the *PP-P* residual from each synthetic seismogram and we distinguish them using superscripts and/or subscripts such as Δt^C, Δt^N, $\Delta t^C_{0.5\,\mathrm{Hz}}$, $\Delta t^N_{0.1\,\mathrm{Hz}}$, . . . , where superscripts *C* and *N* indicate traveltimes measured with and without the crustal correction, respectively, and the subscript indicates the corner frequency.

Even after lowpass filtering the synthetic *PP* waveform with the crustal correction agreed well with the observed *PP* (Figs 2d–f and 3d–f). The agreement was not as good if no crustal correction was applied (Figs 2a–c and 3a–c), resulting in a lower correlation coefficient. Because the precursors and post-cursors were separated from the main *PP* phase in time on the 0.5 Hz lowpass filtered seismogram, the correlation coefficient was mainly controlled by the main *PP* of large amplitude. The measured *PP-P* residuals $\Delta t^C_{0.5\,\mathrm{Hz}}$ and $\Delta t^N_{0.5\,\mathrm{Hz}}$ were, therefore, almost the same, and equal to approximately zero. Upon application of the 0.1 or 0.05 Hz lowpass filter, however, the precursors and post-cursors interfered with the main *PP* waveform. Such interference causes an apparent time-shift of the main *PP* lobe (Fukao *et al.* 2003), which produced a significant bias in the *PP-P* time measurement. The absolute values of ΔT^N increased as the corner frequencies of lowpass filtering decreased and $\Delta t^N_{0.05\,\mathrm{Hz}}$ is -1.47 s (solid PREM) or -0.97 s (PREM) with respect to $\Delta t^N_{0.5\,\mathrm{Hz}}$. In contrast, the *PP-P* times $\Delta t^C_{0.1\,\mathrm{Hz}}$ and $\Delta t^C_{0.05\,\mathrm{Hz}}$ were not very different from $\Delta t^C_{0.5\,\mathrm{Hz}}$, and even $\Delta t^C_{0.05\,\mathrm{Hz}}$ was only -0.2 s. For PREM, $|\Delta t^N_{0.1\,\mathrm{Hz}}|$ was slightly smaller than $|\Delta t^C_{0.1\,\mathrm{Hz}}|$, however, the discrepancy between the observed *PP* waveform and synthetic one without the crustal correction was too large to recognize that they are the same phase.

Our experiment has shown that measured *PP-P* times tend to be smaller than the predicted times when the synthetic *PP* is constructed without a crustal correction and the bias increases as a lower frequency filter is used. The bias can be reduced significantly by the crustal correction and the measured *PP-P* times with the correction are consistent with the predicted values regardless of cut-off frequencies of lowpass filtering.

3 SYNTHETIC EXPERIMENT

In this section, we estimated how much the interference of crustal reverberations can apparently shift the main *PP* in time. The apparent time-shift was obtained by comparing the synthetic *PP* waveforms synthesized from a *P* waveform with and without the convolution with a crustal response. The synthetic *PP* waveform without the convolution was equivalent to reflection at a surface where there is no crustal layer underneath. We obtained the synthetic *PP* waveform, regardless of the crustal structure under its bounce point, by applying a convolution with the crustal responses for the corresponding crustal structures. Therefore, we were able to estimate the time-shifts for various models easily. For the following experiments, the *PP* waveforms were synthesized from the *P* waveform calculated for the solid PREM using the DSM as in the previous section.

First, we investigated the time-shift as a function of crust thickness. The crust used here consisted of the upper and lower crust, and their thickness ratio and physical properties are the same as the solid PREM (Table 1). As shown in Fig. 4 negative apparent time-shifts increase as crust thickness increases. If the crust is so thick that reverberations do not interfere with the main *PP*, there should be no time-shift. Therefore, the time-shift versus thickness curve has its minimum at a thickness that depends on the cut-off frequency. In this experiment, the minimum occurs at thicknesses of about 3,

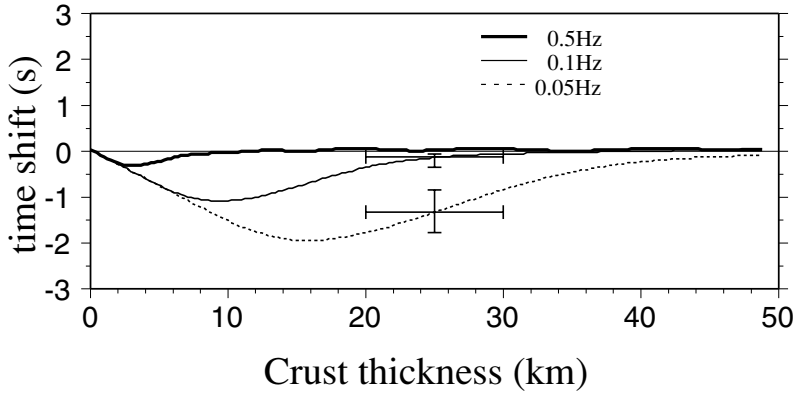

Figure 4. Apparent time-shifts as a function of crust thickness. See text for the crustal model. The estimations using lowpass filtered waveforms with three different corners at 0.5, 0.1 and 0.05 Hz are shown in thick, thin and dotted lines, respectively. The cross-bars indicate possible measurement errors in case of an inappropriate crustal correction. See the text for the details.

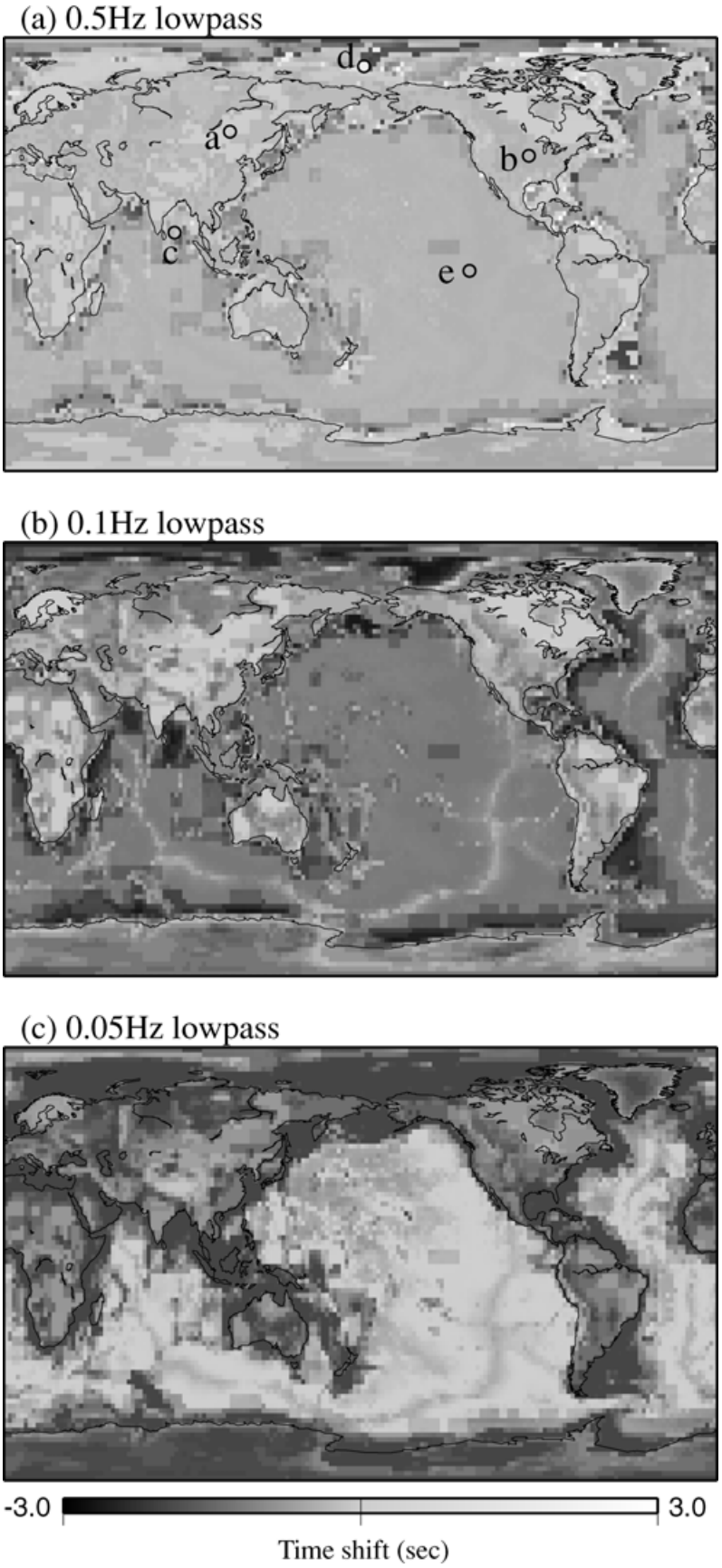

Figure 5. Apparent time-shifts estimated from the crustal model CRUST2.0. The value of the time-shift is plotted on the hypothetical *PP* bounce point. The estimations using lowpass filtered waveforms with three different corners at 0.5, 0.1 and 0.05 Hz are shown at the top, middle and bottom, respectively.

9.5 and 15 km for the 0.5, 0.1 and 0.05 Hz corner frequencies, respectively, where the apparent time-shift was −0.3, −1.1 and −1.9 s, respectively. This suggests that the effect of the crust is significant for long period seismograms.

The negative apparent time-shift can be explained by the polarities of the reverberations. Fig. 1(b) shows the crustal responses for the solid PREM (Fig. 1b), where the precursors had the same polarities as the main *PP* wave while the post-cursors had the opposite polarities. If a wave with such precursors and post-cursors is lowpass filtered, the overall wave apparently shifts negatively in time, resulting in an apparent negative time-shift of the *PP* waveform.

In the same manner as the above synthetic experiment, we estimated the apparent time-shifts of *PP*, using a more realistic 2° × 2° crustal model: CRUST2.0 (Bassin *et al.* 2000). These shifts indicate how much *PP-P* time measurements are biased without the crustal correction if CRUST2.0 is representative of the crust. Fig. 5 shows the estimated time-shift plotted on the *PP* bounce point. The time-shifts were negative in most regions as expected. In the continental regions the time-shift decreased as the corner frequency of the lowpass filter was lowered. For the continental *PP* bounce points, the averages of the time-shifts estimated with the 0.5, 0.1 and 0.05 Hz lowpass filtered waveforms were −0.25, −0.59 and −1.37 s, respectively. In the oceanic regions, the relation between the corner frequencies and the time-shifts was more complicated, while the amounts of time-shift were small in the middle of the oceans.

Fig. 6 shows five examples of synthetic *PP* waveforms. Their bounce points are indicated by circles in Fig. 5 and the crustal structures are listed in Table 2. The waveforms in Figs 6(a) and (b) are from continental bounce points and are very similar to each other. The time-shifts are, however, significantly different. Differences in the waveform cannot be recognized visually. In the cases of reflection under the ocean (Figs 6c, d and e), the amplitude of the crustal reverberations can be larger than that of the main *PP*, which makes the resultant *PP* waveforms complex. On the 0.5Hz lowpass filtered waveform, it is often hard to recognize the main *PP* from such large crustal reverberation signals unless crustal corrections have been made. The complexity of the waveform may lead to a misidentification of the main *PP* phase, resulting in a large time-shift, which could even be positive (Fig. 6d). Such a misidentification can be avoided if the appropriate crustal correction is applied.

4 APPLICATION TO REAL DATA

We applied the method of *PP-P* differential traveltime measurement with crustal correction to real seismograms. We used broad-band seismograms provided by the Incorporated Research Institutions for Seismology (IRIS), Data Management Center (DMC) for the period from 1996 to 1998. We avoided data at epicentral distances where *P* or *PP* triplications from the upper-mantle discontinuities take place and where the *P* waves diffract along the core–mantle

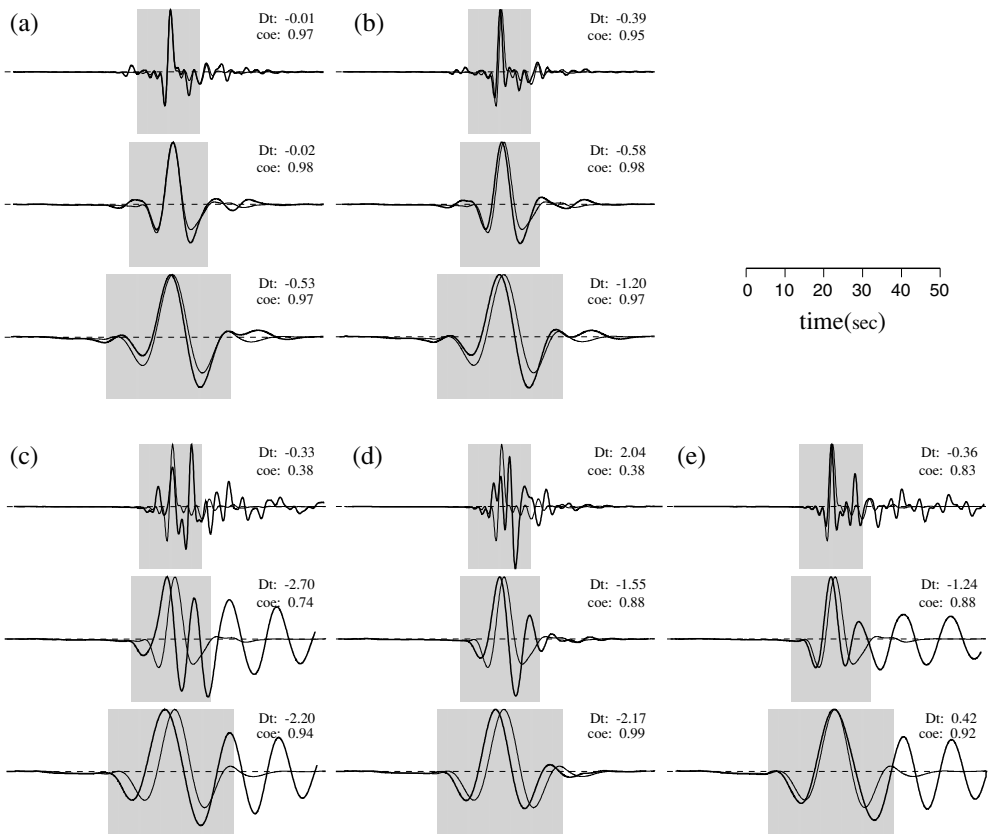

Figure 6. Five examples of the 0.5, 0.1 and 0.05 Hz lowpass filtered synthetic *PP* waveforms representing the apparent time-shifts. The syntheses with the crustal correction (thick lines) are superposed on those without the crustal correction (thin lines). The locations where the crustal structures were used for the crustal correction are shown in Fig. 5(a) and their properties are listed in Table 2. The apparent time-shift (Δt) measured using the cross-correlation method and maximum correlation coefficient are indicated at the top right of each diagram. The shaded area is the window for the cross-correlation that fixed on the synthesis without the crustal corrections.

Table 2. Five crustal structures used to synthesize the *PP* waveforms shown in Fig. 6

		Sea water	Soft sed.	Hard sed.	Upper crust	Mid. crust	Lower crust
(a)	V_P	1.50	2.50	4.00	6.20	6.40	6.80
	V_S	0.00	1.20	2.10	3.60	3.60	3.80
	ρ	1.02	2.10	2.40	2.80	2.85	2.95
	H	0.00	0.00	0.00	13.0	12.0	12.0
(b)	V_P	1.50	2.50	4.00	6.20	6.60	7.30
	V_S	0.00	1.20	2.10	3.60	3.70	4.00
	ρ	1.02	2.10	2.40	2.80	2.90	3.10
	H	0.00	0.00	1.00	16.0	15.0	9.0
(c)	V_P	1.50	2.30	3.50	5.00	6.60	7.10
	V_S	0.00	1.20	1.80	2.50	3.65	3.90
	ρ	1.02	2.20	2.30	2.60	2.90	3.05
	H	3.678	1.50	3.50	1.70	2.30	2.50
(d)	V_P	1.50	2.30	3.20	5.00	6.60	7.10
	V_S	0.00	1.10	1.60	2.50	3.65	3.90
	ρ	1.02	2.20	2.40	2.60	2.90	3.05
	H	1.497	1.50	0.50	1.70	2.30	2.50
(e)	V_P	1.50	1.80	3.20	5.00	6.60	7.10
	V_S	0.00	0.80	1.60	2.50	3.65	3.90
	ρ	1.02	1.70	2.30	2.60	2.90	3.05
	H	4.497	0.07	0.00	1.70	2.30	2.50

The crust model consists of five layers: sea water, soft sediment, hard sediment, upper crust, middle crust and lower crust. V_P, V_S, ρ and H represent *P*-wave velocity (km s^{-1}), *S*-wave velocity (km s^{-1}), density (g cm^{-3}) and thickness (km), respectively.

boundary. We also omitted data where *sP* waves arrived near *PP*. We used CRUST2.0 for the crustal correction at *PP* bounce points. For the surface relief we referred to the finer (2 min mesh) data of ETOPO2 provided by the National Geophysical Data Center because both Fukao *et al.* (2003) and our experiments have shown a significant impact of sea water reverberations on the *PP* waveform. If the bounce point was identified as one under the ocean by ETOPO2, the sea water layer was placed at the top of the solid crust in CRUST2.0 to calculate the crustal response function. The window for the cross-correlation was fixed on the synthetic *PP* waveform, so that the time of maximum amplitude is centered in it, and its width varied according to the corner frequency of lowpass filtering (16, 32, and 64 s for 0.5, 0.1, and 0.05 Hz corner frequency, respectively). After a semi-automatic measurement using the cross-correlation method, we visually inspected the observed and synthetic waveforms mutually superposed in the maximum correlation as shown in Fig. 7 and then assigned a grade of A, B, or C, based on our confidence in that measurement. We obtained six values for the *PP-P* time, T, for each seismogram, as described in the previous section, according to the three cut-off frequencies (0.5, 0.1 and 0.05 Hz) of the lowpass filtering for each of which the synthetic *PP* was calculated with or without the crustal correction. We used the same superscripts and subscripts as used in the synthetic experiment.

Fig. 7 shows examples of the *PP-P* time measurements for the 1996 event near New Guinea recorded at KBS. The *PP*-wave bounce point was located under a continent. As observed in the synthetic experiment (Fig. 5), T^N became smaller as lower frequency filters were applied, while T^C remained almost unchanged with the different corner frequencies, demonstrating that the correction works effectively.

So far, we have obtained 1928 ($T^C_{0.5\,\mathrm{Hz}}$), 3500 ($T^C_{0.1\,\mathrm{Hz}}$), 4772 ($T^C_{0.05\,\mathrm{Hz}}$), 1607 ($T^N_{0.5\,\mathrm{Hz}}$), 3038 ($T^N_{0.1\,\mathrm{Hz}}$) and 4313 ($T^N_{0.05\,\mathrm{Hz}}$) *PP-P* measurements. The number of T^C measurements is larger than that of T^N, regardless of the cut-off frequency. The better correlation between the observed *PP* and synthetic *PP* with the crustal correction leads to an increase in the number of measurements. Fig. 8 shows histograms of *PP-P* residuals with respect to the IASP91 model (Kennett & Engdahl 1991). The measured differential times have been corrected for the Earth's ellipticity (Dziewonski & Gilbert 1976) and the altitude of the *PP* bounce point. The average of T^C depends little on the corner frequency of the lowpass filter, whereas the average of T^N decreases as lower frequency filters are applied. This indicates that biases caused by interference from crustal reverberations have been effectively reduced by correcting for such an effect. Thus, the significance of the crustal correction is supported not only by the synthetic experiment, however, also by thousands of real measurements.

To investigate how the value of $T^N - T^C$ is related to the crustal structure, we divided the measured data into 16200 subsets so that the bounce points of *PP* in each subset were located within the same $2^\circ \times 2^\circ$ cell. These cells correspond to the grid of the crustal model CRUST2.0. Fig. 9 shows the average of $T^N - T^C$ for each subset plotted in the center of the cells. Cells involving more than two *PP* reflections are plotted. The values of $T^N - T^C$ are negative and their absolute values are small under the middle of continents and oceans, and are large near continent–ocean borders. This tendency was also observed in the synthetic experiment (Fig. 5).

5 DISCUSSION

We have shown that interference of the crustal reverberations with the incident *PP* shifts the *PP* lobe negatively in time and that this shift depends on the applied filter frequencies. By applying a crustal correction, we have been able to obtain consistent *PP-P* times among lowpass filtered seismograms with different corner frequencies. Indeed, the application of the crustal correction using CRUST2.0 has enabled us to obtain consistent values among lowpass filtered seismograms with three different (0.5, 0.1 and 0.05 Hz) corner frequencies. This consistency demonstrates that the crustal correction has been made efficiently and possible biases resulting from interferences of crustal reverberations are insignificant on the whole.

If the correction were not appropriate, however, the measurement value might contain an error. We examined the error arising from inappropriate use of the crust-thickness value. Because the apparent time-shift is caused by the interference of reverberations with the main *PP*, it depends on the arrival times of the reverberations relative to the main *PP*. The arrival times of the reverberation are controlled mainly by the depths of crustal discontinuities rather than by velocity perturbations of several per cent within the crust. We determined the apparent time-shift for the simple solid-PREM-like crust with various thicknesses in Section 3. The result is shown in Fig. 4 and the time-shifts at 25 km thickness are 0.03, −0.12 and −1.32 s for the 0.5, 0.1 and 0.05 Hz corner frequencies, respectively. If crust thicknesses differing by ±5 km (shown by lateral bars in Fig. 4) are used for the correction, Fig. 4 indicates that the measured values would contain errors of approximately ±0.03, 0.2 and 0.5 s for the 0.5, 0.1 and 0.05 Hz lowpass filtered seismograms, respectively.

Background noise is another factor that introduces error to a measurement. The amplitude of the crustal reverberation is

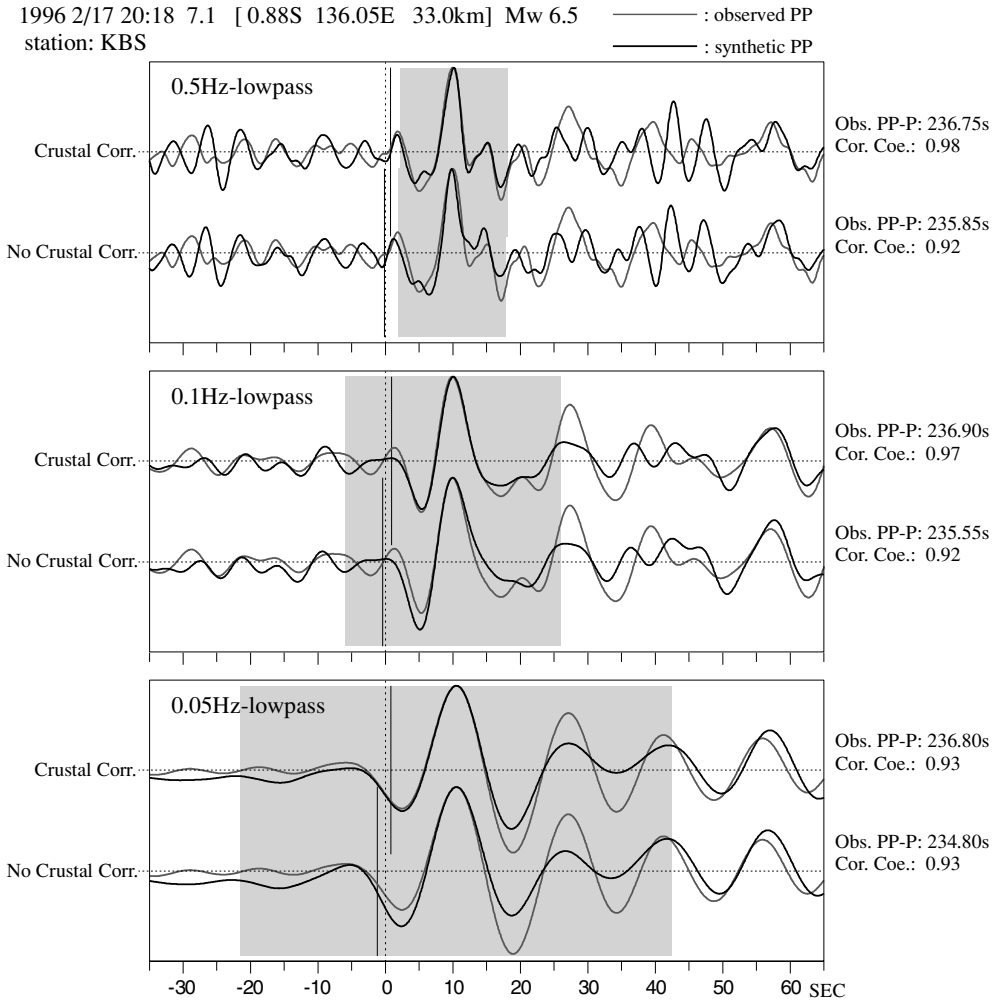

Figure 7. Examples of *PP-P* differential time measurements for the 1996 Feb 17 event near New Guinea, recorded at station KBS. The seismogram was lowpass filtered with three different corner frequencies (top, middle and bottom are 0.5, 0.1 and 0.05 Hz, respectively). In each panel the dark lines at the top and bottom are the synthetic *PP* waveforms constructed with and without crustal correction, respectively, which are superposed on the observed *PP* waveform (thin line) at a time of maximum correlation. The *PP* arrival time predicted from IASP91 was set to zero in time. The IASP91-predicted *P* arrival time was marked on the *P* waveform before synthesizing the *PP* waveform and is shown by the vertical solid line that indicates the *PP-P* residual with respect to IASP91.

sometimes as large as the background noise in a real seismogram. For the example seismogram shown in Fig. 7, the signal-to-noise ratio is approximately 3 and the noise may have caused some apparent time-shift which may obscure the effect of the crustal reverberations. To evaluate the influence of noise, we added noise to the observed seismogram calculated for the solid PREM and then measured a *PP-P* time using the same method as used to produce Fig. 2. We created a thousand sets of synthetic noise data with their spectra consistent with the typical noise model of the Global Digital Seismograph Network and with a maximum amplitude of approximately one third of the *PP* phase. In Fig. 10, the frequency distributions of the *PP-P* residuals measured without the crustal correction are shown in black and those with the crustal correction in light grey. The mean values are almost the same as the values obtained from noise-free seismograms. The standard deviations are 0.16 and 0.20 s for the 0.1 and 0.05 Hz lowpass filtered seismograms, respectively, and are smaller than the observed time-shifts. This indicates that there is a statistically meaningful difference between the *PP-P* times measured with and without the crustal correction.

In our crustal correction we assumed that the crust was laterally stratified. The real crust, however, has 3-D variations, making the effects of crustal reverberations frequency-dependent. The Fresnel zones of 0.5 and 0.05 Hz *PP* waves at an epicentral distance of 80° are approximately 5° × 5° and 15° × 15° wide, centered around the geometrical ray path. The typical pattern sizes of estimated apparent time-shifts shown in Fig. 4 are not less than the Fresnel zone size. Therefore, the 3-D effects are expected to be small in most cases. The effects are, however, expected to be complicated near the coastline where crust thicknesses change steeply (Okamoto 1993). In such regions our correction may not work efficiently.

The crustal correction should, also, be useful for measuring a *PP* traveltime (residual) by cross-correlating the observed *PP* waveform with the synthetic *PP* waveforms calculated on the reference Earth model (e.g. Ritsema & van Heijst 2002). In this case, the synthetic *PP* waveform should be deconvoloved with the response of the crustal model used in the synthetic seismogram and then convolved with the response of an appropriate crustal model at the *PP* bounce point. The same procedures may be taken for the receiver (and the source in case of a shallow event) as well as for the bounce point. The

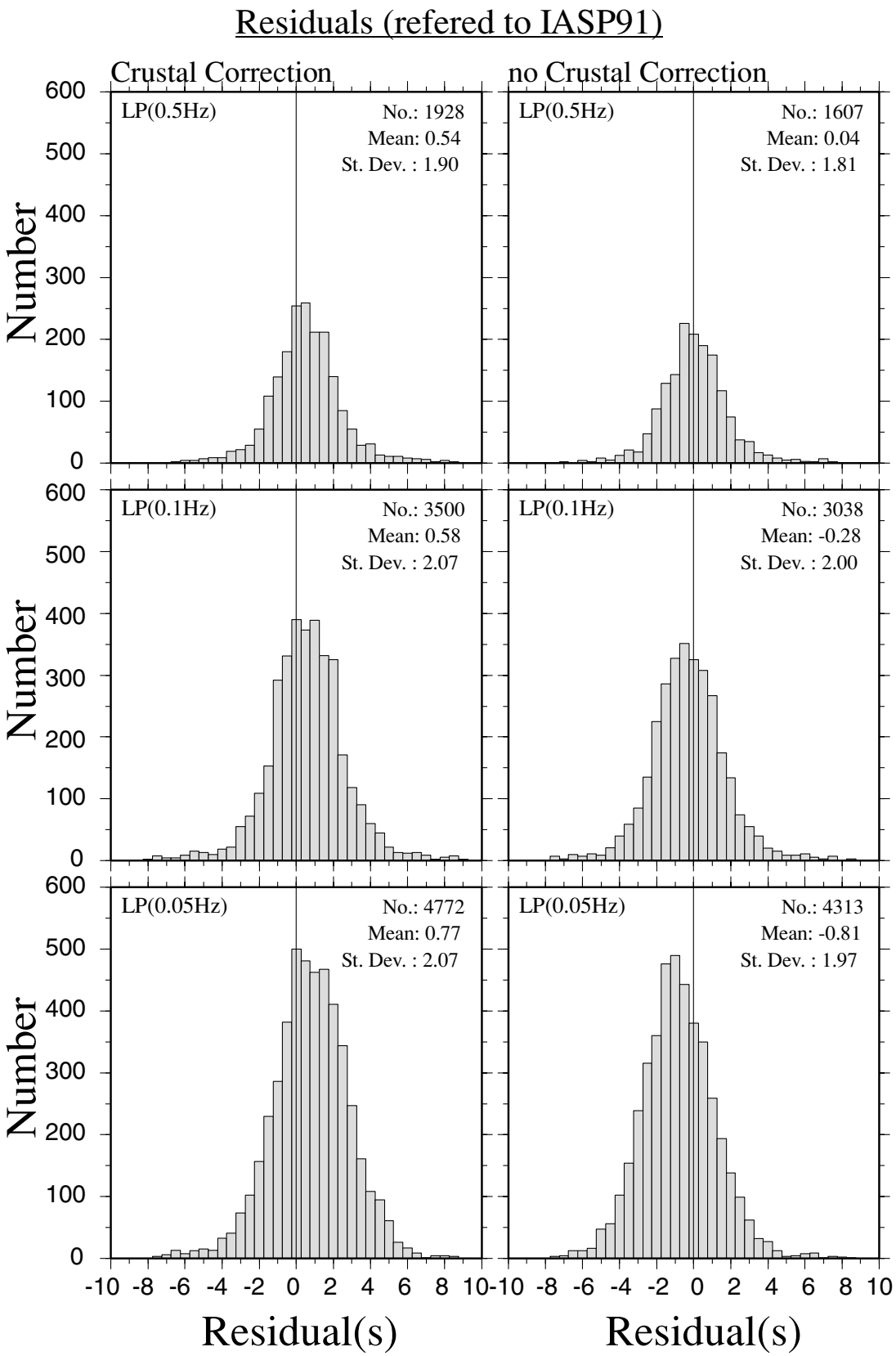

Figure 8. Histograms of *PP-P* time residuals with respect to IASP91, from measurements with (left) and without (right) crustal correction, using lowpass filtering with three different corner frequencies (top, middle and bottom are 0.5, 0.1 and 0.05 Hz, respectively). The total number of data, the average and the standard deviation are shown at the top right corner of each diagram.

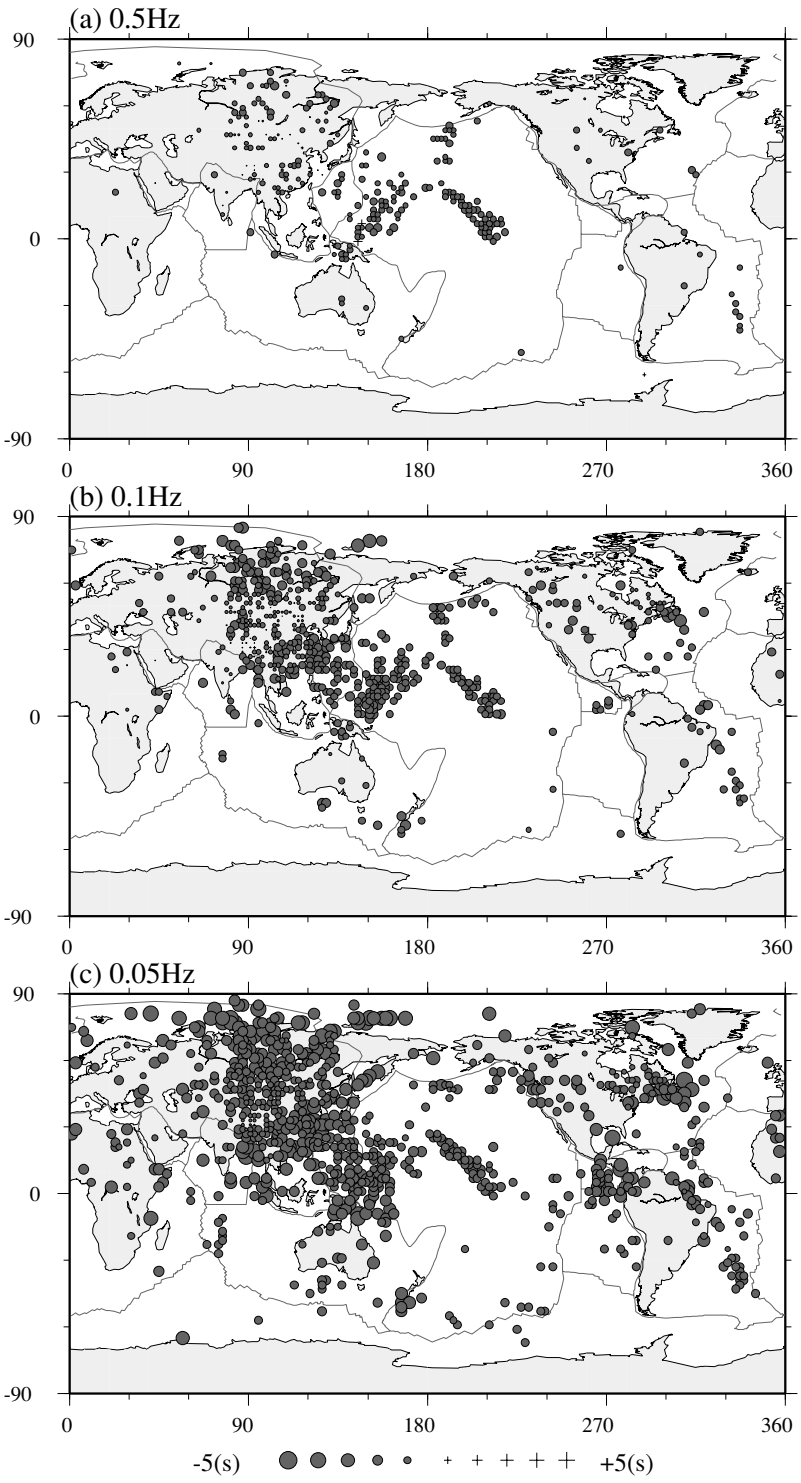

Figure 9. Distribution of cell averages of $T^N - T^C$. The cell size is $2^\circ \times 2^\circ$. Refer to the text for explanation of $T^N - T^C$.

crustal correction can be also applied to measure *SS* traveltimes and *SS*-*S* differential time measurements (Woodward & Masters 1991; Masters *et al.* 2000).

Even if measurements were made without a crustal correction, the measured (differential) traveltimes may be corrected to a first approximation if the filter response is known. We can compute the values of the apparent time-shift for a crustal structure model at a *PP* (*SS*) bounce point as a function of ray parameter using synthetic seismograms, as shown in Fig. 5. The corresponding values can then be applied to correct (differential) traveltimes measured without the crustal correction.

ACKNOWLEDGMENTS

The authors are grateful to an anonymous reviewer for useful comments. The authors thank H. Ohno for managing the *PP-P*

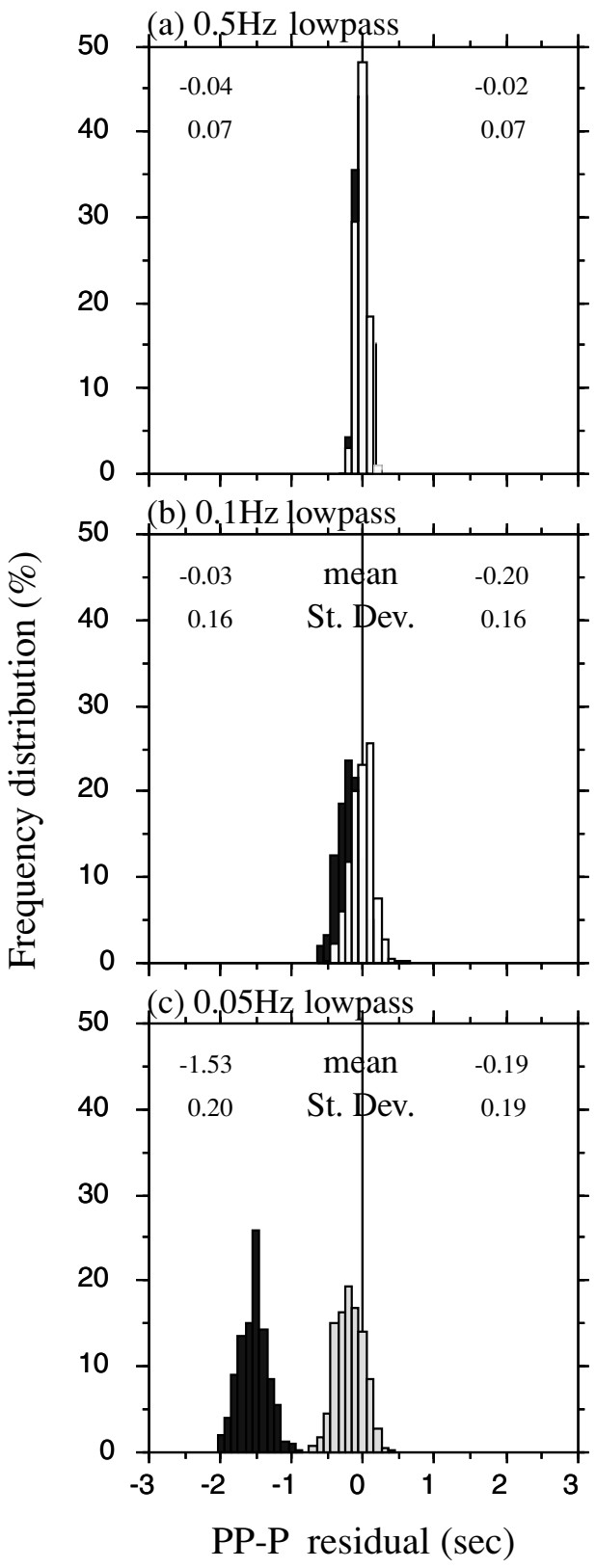

Figure 10. Histograms of *PP-P* time residuals measured from synthetic seismograms to which 1000 sets of noises were added. The measurements with and without crustal correction are shown in light gray and black, respectively, with dark gray for the overlap portions. The values of the means and standard deviations for the measurements with and without crustal correction are indicated at the top right and top left, respectively.

differential traveltime data measured in this study. All figures have been produced using GMT software of Wessel & Smith (1995).

REFERENCES

Bassin, C., Laske, G. & Masters, G., 2000. The current limits of resolution for surface wave tomography in North America, *EOS, Trans. Am. geophys. Un.,* **81,** F897.

Dziewonski, A.M. & Anderson, D.L., 1981. Preliminary reference Earth model, *Phys. Earth planet. Int.,* **25,** 297–356.

Dziewonski, A.M. & Gilbert, F., 1976. The effect of small aspherical perturbations on traveltimes and re-examination of the corrections for ellipticity, *Geophys. J. R. astr. Soc.,* **44,** 7–16.

Fukao, Y., To, A. & Obayashi, M., 2003. Whole Mantle P-wave Tomography Using P and PP-P data, *J. geophys. Res.,* doi: 10.1029/2001 JB000989.

Haskell, N.A., 1962. Crustal reflection of plane P and SV waves, *J. geophys. Res.,* **67,** 4751–4767.

Kennett, B.L.N. & Engdahl, E.R., 1991. Travel times for global earthquake location and phase identification, *Geophys. J. Int.,* **105,** 429–465.

Masters, G., Laske, G., Bolton, H. & Dziewonski, A.M., 2000. The relative behavior of shear velocity, bulk sound speed, and compressional velocity in the mantle: Implications for chemical and thermal structure, p. 63–87, in *Earth's Deep Interior, Mineral Physics and Tomography, From the Atomic to the Global Scale*, Geophysical Monograph **117**, 289, eds Karato, S., *et al.*, AGU, Washington, DC.

Okamoto, T., 1993. Effects of sedimentary structure and bathymetry near the source on teleseismic P waveforms from shallow subductuin zone earthquakes, *Geophys. J. Int.,* **112,** 471–480.

Paulssen, H. & Stutzmann, E., 1996. On PP-P differential travel time measurements, *Geophys. Res. Lett.,* **23,** 1833–1836.

Ritsema, J. & van Heijst, H.J., 2002. Constraints on the correlation of P- and *S*-wave velocity heterogeneity in the mantle from P, PP, PPP and PKPab traveltimes, *Geophys. J. Int.,* **149,** 482–489.

Takeuchi, N., Geller, R.J. & Cummins, P.R., 1996. Highly accurate P-SV complete synthetic seismograms using modified DSM operators, *Geophys. Res. Lett.,* **23,** 1175–1178.

Wessel, P. & Smith, W.H.F., 1995. New version of the generic mapping tools released, *EOS, Trans. Am. geophys. Un.,***76,** 329.

Woodward, R.L. & Masters, G., 1991. Global upper mantle structure from long-period differential travel times, *J. geophys. Res.,* **96,** 6351–6377.